Nanostructured electrocatalysts with tunable activity and selectivity

Hemma Mistry[1,2], Ana Sofia Varela[3], Stefanie Kühl[3], Peter Strasser[3] and Beatriz Roldan Cuenya[2]

Abstract | The field of electrocatalysis has undergone tremendous advancement in the past few decades, in part owing to improvements in catalyst design at the nanoscale. These developments have been crucial for the realization of and improvement in alternative energy technologies based on electrochemical reactions such as fuel cells. Through the development of novel synthesis methods, characterization techniques and theoretical methods, rationally designed nanoscale electrocatalysts with tunable activity and selectivity have been achieved. This Review explores how nanostructures can be used to control electrochemical reactivity, focusing on three model reactions: O_2 electroreduction, CO_2 electroreduction and ethanol electrooxidation. The mechanisms behind nanoscale control of reactivity are discussed, such as the presence of low-coordinated sites or facets, strain, ligand effects and bifunctional effects in multimetallic materials. In particular, studies of how particle size, shape and composition in nanostructures can be used to tune reactivity are highlighted.

The electrocatalytic conversion of renewable resources, such as CO_2 or biomass, to chemicals, fuels and electrical energy is a promising means to meet the most urgent technological goals of our time; namely, clean energy production and environmental remediation. Key technologies are based on the development of hydrogen- or hydrocarbon-based fuel cells that could allow us to divest from fossil fuels and close the carbon cycle via the conversion of CO_2 to useful products. Some of the current challenges for modern electrocatalysis are to improve O_2 conversion reactions (namely, the oxygen reduction reaction (ORR) and the oxygen evolution reaction (OER)), hydrocarbon conversion reactions for direct alcohol fuel cells (for methanol, ethanol and formic acid oxidation) and CO_2 electroreduction. However, new catalytic materials are needed that are highly efficient, stable and scalable.

The past few decades have seen tremendous advances in the development of novel nanostructured catalysts for electrochemical reactions. Nanomaterials often show enhanced activity compared with bulk materials owing to their unique morphological, electronic and chemical surface properties. These properties can be carefully tuned to modify the activity and selectivity of electrocatalytic reactions. The size of the nanoparticle can be used to control the number of low-coordinated sites on the catalyst surface, which may influence reactant binding strength. The shape of the nanoparticle can be used to control the presence of certain facets that may be highly favourable for a particular reaction. The size and shape of the catalyst may also influence the stability of oxide species at the surface, which may, in turn, determine the activity or selectivity for a reaction. In multimetallic catalysts, more complex mechanisms may come into play. For example, geometric or strain effects may alter surface properties by distorting the atomic arrangement on the catalyst surface. In addition, electronic or ligand effects can cause a shift in the *d*-band centre of metal atoms at the catalyst surface, leading to altered binding of reactants and intermediates. Furthermore, different metal atoms may enhance different steps in a reaction through a bifunctional mechanism or provide an optimal ensemble of active sites on the catalyst surface.

Electrocatalytic reactions are highly complex because of the interplay among the solid catalyst, the electrolyte, and gas- and liquid-phase reactants and products. To understand the mechanism behind the improved catalytic ability of nanomaterials and to derive the design principles necessary to make better catalysts, studies of model systems are vital. For key energy conversion reactions, studies of single-crystal catalysts have provided an important insight into the structure sensitivity, while advances in nanomaterial synthesis have allowed further understanding of structure–property relationships based on novel nanocatalysts with a well-defined size, shape and composition. In addition to the controlled synthesis and characterization of catalytic activity and selectivity, cutting-edge characterization techniques,

[1]*Department of Physics, University of Central Florida, Orlando, Florida 32816, USA.*
[2]*Department of Physics, Ruhr-University Bochum, 44780 Bochum, Germany.*
[3]*Department of Chemistry, Chemical Engineering Division, Technical University Berlin, 10623 Berlin, Germany.*

Correspondence to P.S. and B.R.C.
pstrasser@tu-berlin.de; Beatriz.Roldan@rub.de

Article number: 16009
doi:10.1038/natrevmats.2016.9
Published online 15 Mar 2016

particularly *in situ* and *in operando* microscopy and spectroscopy, can reveal dynamic changes in the structure, morphology and chemical state of nanocatalysts during a reaction. Furthermore, theoretical and computational studies have allowed remarkable insight into reaction mechanisms, which complement experimental findings.

In this Review, we assess our current knowledge of tunable activity and selectivity in electrocatalytic processes that are controlled through the rational design of nanomaterials with well-defined structures. We focus on three key reactions for electrocatalytic energy production: the ORR, CO_2 electroreduction and the electrooxidation of ethanol. Heterogeneous metal and metal oxide catalysts were selected as model systems. For each reaction, the most promising catalysts are discussed, in addition to the structure-dependent mechanisms behind their enhanced performance. Such structural parameters include nanocatalyst size, shape, spacing, crystallographic orientation, chemical state, support material and composition (that is, the addition of a secondary or ternary metal). Finally, we discuss the remaining challenges and the outlook of future research directions.

Oxygen reduction reaction

The electrocatalytic ORR is a challenging reaction in metal–air battery and fuel cell technology (for example, polymer electrolyte membrane (PEM) fuel cells) because of its slow rate and high overpotentials[1–3]. The volume of research, in the context of electrochemical energy technologies, conducted on the ORR over the past several decades[3–11] has been tremendous. In PEM fuel cells, the catalysts at the anode and cathode typically consist of Pt nanoparticles supported on conducting carbon (for example, carbon black[1]), which is the reason that this Review highlights aspects of activity and selectivity in nanostructured Pt-based catalysts.

Depending on the electrode material, the pathway of the ORR can be either the direct four-electron reduction to H_2O (equation 1) or the competitive, indirect pathway via H_2O_2 as an intermediate (equations 2 and 3).

$$O_2 + 4H^+ + 4e^- = 2H_2O \quad E_0 = +1.23\ \text{V vs RHE} \quad (1)$$
$$O_2 + 2H^+ + 2e^- = H_2O_2 \quad E_0 = +0.695\ \text{V vs RHE} \quad (2)$$
$$H_2O_2 + 2H^+ + 2e^- = 2H_2O \quad E_0 = +1.78\ \text{V vs RHE} \quad (3)$$

Early isotope measurements revealed that H_2O_2 formation occurs without O–O bond cleavage, whereas H_2O formation requires the O–O bond to break[12,13]. Much experimental and computational effort has been invested to investigate the detailed ORR mechanism on various electrode materials, revealing that the binding energy of oxygenate intermediates on the catalyst surface may serve as a suitable controlling parameter for ORR selectivity and activity[14–16]. According to these studies, the two-electron process is predominantly catalysed on Hg, Au (except Au(100) in alkaline solution)[17], graphite and most metal oxides. By contrast, the four-electron pathway predominantly occurs on pure Pt as well as Pt-based alloys, resulting in H_2O as the main product[12].

In general, the activity and selectivity of the ORR can be tuned by exploiting electronic effects and/or support-induced surface-lattice strain. An atomic neighbourhood of dissimilar atoms and surface-lattice strain[18,19] both shift the energetic *d*-band centre of catalytic materials, leading to altered binding strengths of reaction intermediates. Such strain effects have been explored[20] for Pt monolayers (MLs) on different single crystals that exert compressive or tensile strain on Pt[19]. Tensile strain induced on Pt MLs causes an upward shift in the Pt *d*-band centre, leading to stronger binding of adsorbed oxygen, which facilitates O–O bond breaking. By contrast, compressive strain causes a downward shift in the Pt *d*-band centre, reducing the propensity of the O–O bond to break but enhancing bond formation between weakly adsorbed reactants, which improves the selectivity for H_2O_2 (REF. 20). Another approach to induce selectivity and stability of Pt-based catalysts in the ORR was reported by Genorio *et al.*[21,22] using chemically modified electrodes. They developed self-assembled MLs of calix[4]arene molecules on extended Pt single-crystal surfaces; the modified surfaces showed 100% selectivity in the presence of H_2 and under conditions relevant for PEM fuel cells. Despite these extensive studies on electrocatalysts for the ORR, many questions remain regarding their structure–property relationships; the most important of these are summarized in the following sections.

Effect of particle size and structure. Particle size effects of Pt and Pt alloys in the ORR, which were first addressed more than two decades ago[23–25], remain the subject of intense study. Particle size effects originate, in part, from the structure sensitivity of individual crystal facets, which has been well studied on Pt single crystals and is strongly dependent on the electrolyte[26,27]. Stepped Pt surfaces exhibit surprising structure effects[26], whereby the strong binding of O atoms on Pt step atoms causes an enhanced ORR rate on neighbouring terrace atoms owing to electronic effects[28]. An overwhelming number of studies have shown that ORR activity of Pt nanoparticles decreases with decreasing nanoparticle size, which is most likely because of strongly adsorbed species on the prevalent undercoordinated Pt active sites[29–32]. One limitation of these studies, however, is their failure to take the selectivity for the ORR into account. As discussed above, although H_2O is the main product on bulk Pt surfaces, catalyst dispersion and mass transport phenomena in nanoscale catalysts[33] may result in strong selectivity for the H_2O_2 intermediate.

Effect of interparticle distance. Several research groups have investigated the effect of interparticle distance on the ORR using nanostructured catalysts with highly controlled spacing. For large Pt nanodiscs, Behm and colleagues[34,35] showed that not only was activity improved on more widely spaced discs, owing to the improved mass transport of O_2 to the catalysts, but also that selectivity shifted to the H_2O_2 intermediate, because its readsorption and further reduction to H_2O were limited. Similar results were found by Zou and colleagues[36,37] for

Pt nanoparticles prepared by micelle encapsulation with controlled spacing. For more closely spaced particles, Arenz and co-workers[38,39] have shown that the overlap of the electrical double layer leads to weaker binding of site-blocking spectator species and, therefore, improved activity for the ORR.

Bimetallic catalysts. As previously mentioned, PEM fuel cell electrodes typically contain nanocatalysts of Pt nanoparticles supported on carbon. In terms of sustainability and cost efficiency, studies on fuel cell catalyst development have focused on the synthesis of new nanostructured electrocatalysts to reduce the Pt content. For example, it is well established that both specific activity and mass activity can be enhanced by alloying Pt with other transition metals such as Ni, Fe or Co (REFS 7,11,13,40). Furthermore, it has been shown that an improvement in activity can be achieved by maximizing the exposure of certain facets using shape-controlled nanoparticles[41–50].

In recent years, several innovative surface and subsurface alloy structural concepts (FIG. 1) have been proposed for active bimetallic ORR catalysts. The most popular are Pt-alloy skin and skeleton catalysts[13,29,51–63], Pt-ML catalysts[20,64–70] and dealloyed Pt core–shell catalysts[49,71–77]. Dealloying Pt-poor bimetallic nanoparticles into core–shell nanoparticles, as illustrated in FIG. 1a, is a very promising approach for reducing the Pt catalyst content while boosting the intrinsic reactivity[71,75,76,78]; the surface catalytic properties can be tuned by controlling various parameters of the synthesis method[71,78]. Dealloyed Pt core–shell structures show higher activity[76,79] and improved stability[79,80] in the ORR than other Pt-rich alloys and standard Pt/C catalysts. The most active and stable performance of a Pt alloy cathode catalyst during a realistic PEM fuel cell test was recently reported using a size-controlled dealloyed $PtNi_3$ core–shell nanoparticle catalyst[79]. Furthermore, Wang *et al.*[66] reported similar, well-defined core–shell nanocatalysts obtained by stepwise Pt-ML depositions on Pd and Pd_3Co nanoparticles with controlled particle sizes (4–5 nm) and an enhanced activity for O_2 reduction. Their results suggested that Pt(111) facets are the most conducive on small particles, even more so if they are moderately compressed.

With regard to the development of catalysts, the surface structure also needs to be considered, because the ORR is a structure-sensitive reaction. For Pt nanoparticles in electrolytes without strongly adsorbing ions (for example, 0.1 M $HClO_4$), the specific activities in the ORR are known to increase in the order of Pt(100) << Pt(111) ≈ Pt(110)[56] owing to electronic effects (that is, the binding strength of reaction intermediates). This is rationalized by their surface geometries and the associated electronic structures — in particular, the *d*-band centre, as established by Nørskov and co-workers[18]. They suggested that ORR catalysis on Pt is limited by strongly adsorbed oxygenated intermediate

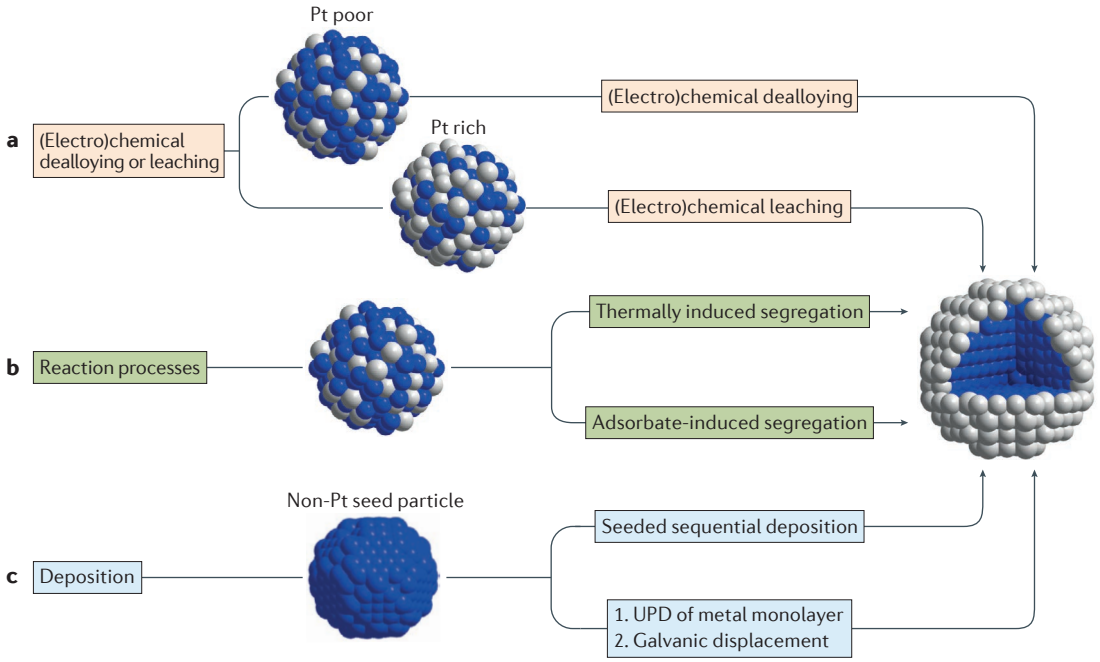

Figure 1 | **Synthesis of Pt-skin, Pt-monolayer and dealloyed Pt-bimetallic nanoparticles with a core–shell structure.** Illustration of basic synthesis approaches for the preparation of core–shell nanoparticle catalysts. **a** | (Electro)chemical dealloying or (acid) leaching results in dealloyed Pt bimetallic core–shell nanoparticles and Pt-skeleton core–shell nanoparticles, respectively. **b** | Reaction process routes generate segregated Pt skin core–shell nanoparticles induced either by strong binding to adsorbates or by thermal annealing. **c** | The preparation of heterogeneous colloidal core–shell nanoparticles or Pt-monolayer core–shell nanoparticles via heterogeneous nucleation and seeded growth, and underpotential deposition (UPD) followed by galvanic displacement, respectively. Adapted with permission from REF. 77, American Chemical Society.

species. A downshift of the Pt *d*-band centre on (110) and (111) facets compared with (100) can weaken such adsorption and, hence, enhance catalytic activity.

The structure sensitivity of PtNi alloys was investigated by Stamenkovic *et al.*[56] using a special Pt-skin structure, which greatly improved ORR activity on the surface of $Pt_3Ni(111)$ facets: ORR activity was 10 times higher than that of a Pt(111) surface and 90 times higher than that of commercial Pt/C nanoparticle catalysts — a so-called dream electrocatalyst. The key characteristic of such a skin surface is an oscillatory near-surface compositional segregation of Pt and Ni across the outermost three layers of the (111) surface: that is, Pt segregated at the outermost surface and Ni segregated at the second layer. The exceptional catalytic activity is related to the combined effects of the atomic structure of the surface (that is, the compact (111) surface) and the composition near the surface (there is high Ni content in the second subsurface layer), which induce a significant downward shift of the *d*-band centre of the outermost Pt surface, thus leading to weakened adsorption of oxygenated intermediate species and high ORR activities. Furthermore, Stamenkovic *et al.*[56] investigated the synergy between the surface geometry and the surface electronic structure of $Pt_3Ni(hkl)$ for the ORR. The order of catalytic activity in the ORR for the different low-index surfaces studied was $Pt_3Ni(100)$ skin < $Pt_3Ni(110)$ skin <<< $Pt_3Ni(111)$ skin, as illustrated in FIG. 2.

Inspired by the exceptional ORR activity reported on an extended Pt-skin (111) surface, different studies have investigated approaches for shaped nanoparticles with well-defined facets for the ORR[43,45–47,81,82]. The impressive performance evolution of shaped PtNi nanoparticles in the past five years is summarized in FIG. 3. For example, the groups of Zou[47] and Yang[45] synthesized octahedral Pt_3Ni nanoparticles based on surfactant-directed reduction in organic solution using tungsten carbonyl or CO as a shape-directing agent. These particles showed a fourfold increase in specific activity compared with pure Pt/C electrocatalysts. Furthermore, a record activity (that is, 17 times higher mass activity and 51 times higher specific activity) was reported by Choi *et al.*[46], who used a slightly modified method to obtain particles with less residual surfactant on the surface. A different, surfactant-free approach for obtaining shaped Pt-alloy nanoparticles was presented by Carpenter *et al.*[42], who used dimethylformamide (DMF) as both the solvent and reductant under solvothermal conditions. The octahedral PtNi nanoparticles that were obtained had diameters in the range of 12–15 nm, and a mass activity 6 times higher and a specific activity 10 times higher than that of Pt/C. Modifying this approach to milder heating conditions, Cui[43] and Gan[44] synthesized octahedral PtNi catalysts that were about 9 nm in diameter and with an ORR mass activity 10 times higher than that of Pt/C by tuning the Pt:Ni composition via the reaction time. They observed an isotropic growth mechanism for both metals, in which the formation of a Pt-rich phase in hexapod-like concave nanocrystals is followed by the deposition of Ni into concave surfaces, resulting in PtNi octahedra with Pt-rich frames and Ni-rich (111) facets.

Chen *et al.*[63] presented nickel-depleted PtNi nanoframes that are even more active than the previously reported octahedral electrocatalysts —with a mass activity 36 times higher and a specific activity 22 times higher than that of Pt/C. They developed a Pt-skin structure from $PtNi_3$ polyhedra, which were converted to Pt_3Ni nanoframes by etching in nonpolar solvents, followed by dispersion of the particles on carbon and subsequent thermal treatment (370–400 °C in argon). Recently, Huang *et al.*[6] reported the record-breaking activity of octahedral PtNi nanoparticles doped with *d* metals (such as V, Cr, Mn, Fe, Co, Mo, W and Re). From this selection of *d* metals, Mo-doped PtNi nano-octahedra (with an edge length of 8 nm) showed 81- and 73-fold enhancements in specific and mass activity in the ORR, respectively, compared with commercial Pt/C catalysts. On the basis of computational data, the origin of this exceptional activity was suggested to be Mo atoms on surface sites near the vertices of the nano-octahedra, which modify the binding strength of reactive intermediates while forming stable Mo–Pt and Mo–Ni bonds.

In summary, the most promising emerging materials concepts for active and selective PEM fuel cell catalysts are dealloyed Pt–Ni core–shell nanocatalysts as well as Pt-based nanoparticles with well-defined geometric shapes. Current studies give testament to the high level of control and craftsmanship that is needed for the chemical preparation of bimetallic nanoparticles with well-defined shapes to achieve high activity in the ORR. However, concrete evidence of sufficient long-term morphological and performance stability under realistic fuel cell conditions is still lacking, making dealloyed cuboctahedral $PtNi_3$ core–shell nanocatalysts — the initial size of which is carefully controlled — the most stable and viable alloy catalysts for PEM fuel cells to date[79].

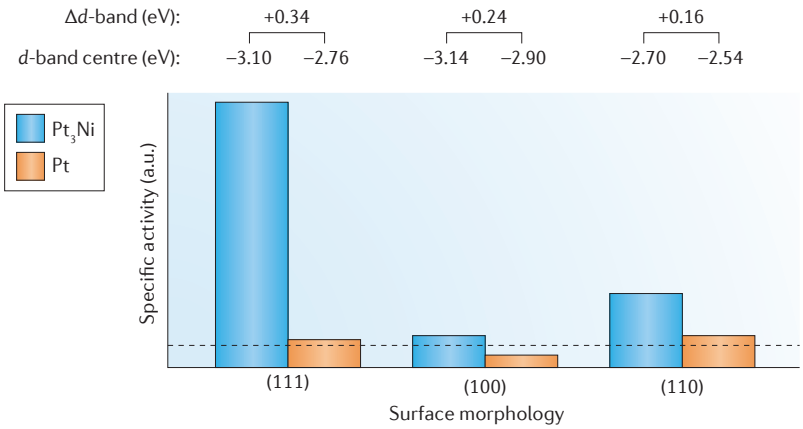

Figure 2 | **Influence of surface morphology and electronic surface properties on the kinetics of the ORR.** Rotating ring disk electrode (RRDE) measurements for the O_2 reduction reaction (ORR) on $Pt_3Ni(hkl)$ surfaces compared with the corresponding Pt(*hkl*) surfaces are shown. The horizontal dashed line marks the specific activity of polycrystalline Pt. Specific activity is the kinetic current density, J_k, measured at 0.9 V versus RHE (reversible hydrogen electrode) (in 0.1 M $HClO_4$ at 333 K with 1,600 rpm). Image is adapted with permission from REF. 56, American Association for the Advancement of Science.

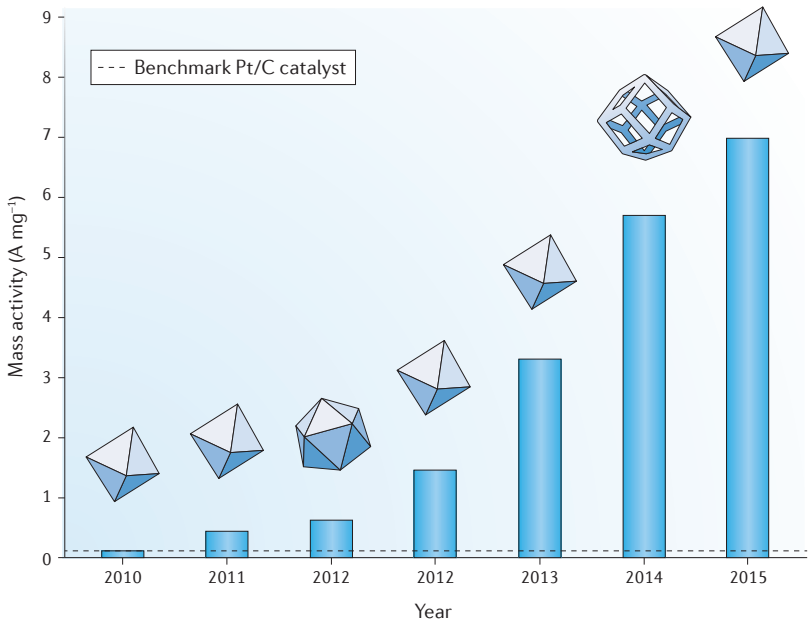

Figure 3 | **Performance evolution of shaped PtNi nanoparticles.** The ever-rising performance/cost ratios (in units of A mg^{-1} (Pt) at +0.9 V_{RHE} iR-corrected electrode potential) for PtNi nanoparticles with octahedral shapes, synthesized by the following groups: Zou[47], Yang[81], Yang[82], Strasser[49], Xia[46], Stamenkovic[63] and Huang[6]. iR, solution resistance; RHE, reversible hydrogen electrode. Image is adapted with permission from REF. 41, American Association for the Advancement of Science.

Dealloyed Pt–Ni core–shell nanoparticle catalysts have already exceeded the US Department of Energy targets for 2017 in terms of stability and activity under realistic automotive fuel cell test conditions.

Carbon dioxide reduction

The electrocatalytic conversion of CO_2 is a promising means to convert CO_2 into useful products such as CO, formate, CH_4, C_2H_4 and alcohols. Compared with other conversion methods, the electrocatalytic reduction of CO_2 is favourable because the reaction occurs under ambient temperature and pressure and in neutral pH. Moreover, because the electrocatalytic splitting of H_2O is intrinsically coupled to the electrocatalytic reduction of CO_2, the latter does not require H_2 as a feedstock[83]. However, CO_2 electroreduction is not yet industrially viable owing to its high overpotential (about −1.0 V) and low selectivity for desirable products compared with the evolution of H_2 (namely, the hydrogen evolution reaction (HER))[84]. Although in recent years there have been many excellent studies of homogeneous catalysts for CO_2 electroreduction[85] as well as other interesting materials, such as MoS_2 (REF. 86), we instead focus on metals and metal oxide catalysts.

Selectivity control in bulk materials. Among all pure-metal catalysts, Cu is unique in that it can selectively produce hydrocarbons[87]. Recently, it has been shown that various metals beyond Cu, as well as solid non-metallic carbon-based catalysts, can also produce hydrocarbons, although at a very low rate[88,89]. The differing selectivity of these metals appears to be due to the binding energies of intermediates from the CO_2 electroreduction reaction on different metal surfaces, with Cu having the optimal electronic structure for the rate-limiting CO protonation step[90–92]. In addition, Cu has an optimal binding energy for COOH and CO intermediates, such that the Cu surface can stabilize COOH without being poisoned by CO (REF. 93). By contrast, metals such as Pt, Ni, Fe and Co are good HER catalysts and may become poisoned at the surface by adsorbed CO*, which explains their low hydrocarbon selectivity[94].

Studies on single crystals have clearly shown that both the reactivity and selectivity of Cu during CO_2 electrochemical reduction are dependent on the crystal facets. The ratio between CH_4 and C_2H_4 depends strongly on the crystal orientation, with Cu(111) favouring the formation of CH_4 and Cu(100) favouring the formation of C_2H_4 (REF. 95). Steps in the crystal surface may improve activity even further by increasing the binding strength of reactants[96]. Indeed, Hori and co-workers[95] showed that steps in the (100) surface increased C_2H_4 selectivity, with an optimal selectivity of 58.9% on Cu(711) surfaces. Both experimental and theoretical studies have been carried out to unravel the mechanism behind the selectivity change on (111) and (100) surfaces. It was found that Cu(100) surfaces facilitate the formation of C_2H_4 through CO dimerization, whereas Cu(111) surfaces favour CO protonation, which is a key step towards CH_4 formation, although C_2H_4 can also be formed via this pathway[97–101].

Selectivity control by nanostructured catalysts. Understanding the structure sensitivity of CO_2 electroreduction over metal nanostructures is highly complex because of the combined effects of properties, such as atomic coordination at the surface, grain boundaries, oxidation states and catalyst dispersion, on the activity and selectivity for several possible products. Nanoparticles often show considerably enhanced activities compared with extended surfaces owing to the presence of low-coordinated atoms that may affect the binding strength of reaction intermediates and, consequently, the selectivity of the reaction. The wide variation in activity and selectivity trends for Cu nanoparticle catalysts for CO_2 electroreduction makes it difficult to extract the mechanism behind their reactivity; therefore, studies on model catalysts are crucial. In a recent study of size-controlled nanoparticles synthesized through reverse micelle encapsulation[102–104], it was determined that the activity towards CO_2 electroreduction over Cu nanoparticles greatly increased for nanoparticles below 5 nm in size owing to the low-coordinated sites on the surface[105] (FIG. 4a). This activity increase was found to originate from increased H_2 evolution and CO formation over smaller nanoparticles. In addition, it was found that the selectivity for hydrocarbons was suppressed, compared with bulk Cu, with decreasing nanoparticle size. By comparison, larger Cu nanoparticles have shown much higher selectivity for hydrocarbons. Some examples include glassy carbon-supported Cu nanoparticles (7 nm)[106] and Cu nanoparticles (12 nm; 40% by weight) supported on Vulcan carbon[107], as shown in FIG. 4b,c. To

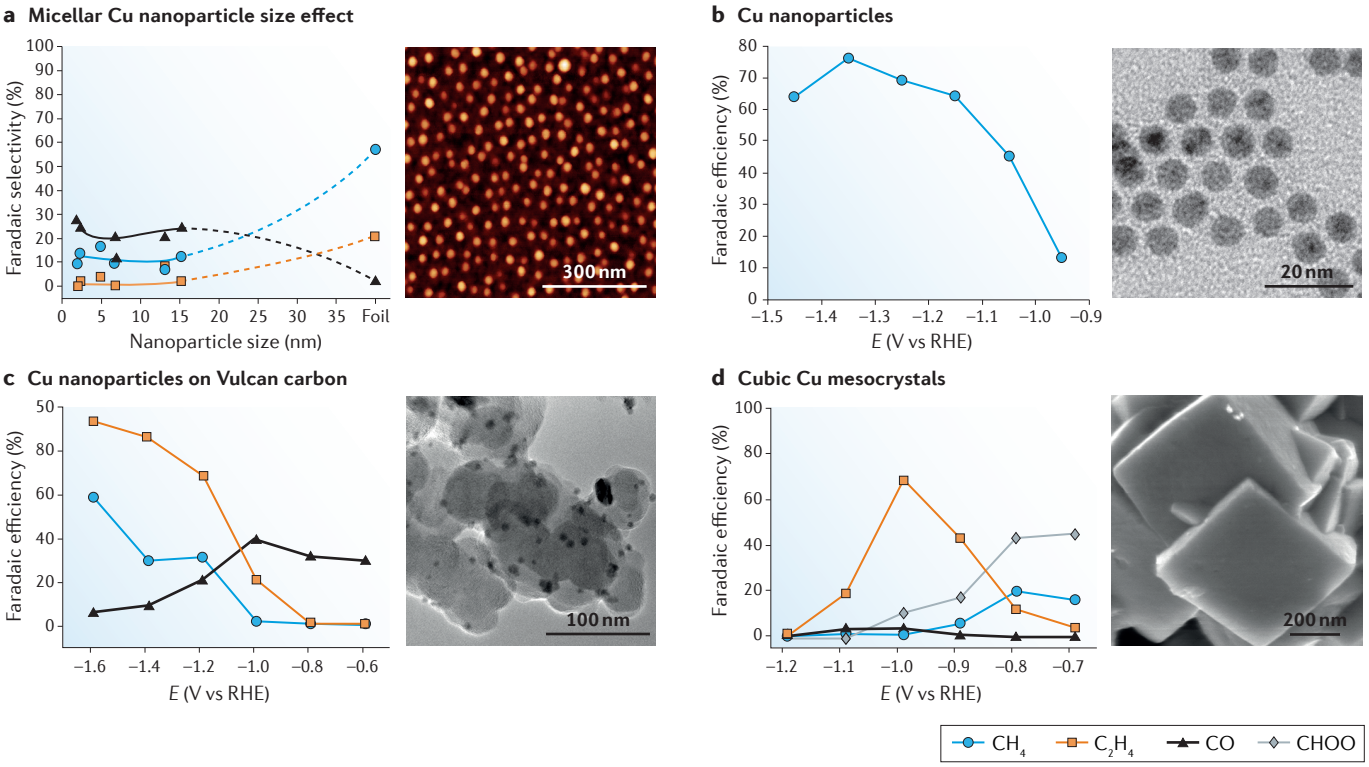

Figure 4 | **Nanostructure effects on the selectivity of Cu catalysts for CO_2 electroreduction. a** | Nanoparticle size-dependent Faradaic selectivity during CO_2 electroreduction over micelle-synthesized Cu nanoparticles supported on glassy carbon at −1.1 V versus RHE (reversible hydrogen electrode). An atomic force microscopy image of micellar Cu nanoparticles is shown on the right. **b** | Faradaic efficiency for CO_2 electroreduction to CH_4 for colloidally synthesized 7-nm Cu nanoparticles supported on glassy carbon. The high-resolution transmission electron microscopy (TEM) image shows the as-prepared nanoparticles. **c** | Faradaic efficiency for Cu nanoparticles (40% by weight) supported on Vulcan carbon. The high-resolution TEM image shows the as-prepared catalyst. **d** | Faradaic efficiency of CuCl-derived Cu mesocrystals. The cubic shape of the initial catalyst is shown in the TEM image. Panel **a** is adapted with permission from REF. 105, American Chemical Society. Panel **b** is adapted with permission from REF. 106, American Chemical Society. Panel **c** is adapted with permission from REF. 107, American Chemical Society. Panel **d** is adapted with permission from REF. 111, Royal Society of Chemistry.

understand size-dependent trends, it is also essential to consider changes in the size and shape of nanoparticles during the reaction. For example, the 7-nm nanoparticles shown in FIG. 4b grow to 23 nm during the reaction, which may explain their different selectivity from the smaller nanoparticles shown in FIG. 4a.

Another critical parameter for Cu nanoparticle catalysts is the interparticle spacing. Mesoscale phenomena, such as interparticle reactant diffusion and readsorption of intermediates, can have a defining role in product selectivity for multistep reactions[35,108]. Indeed, Mistry *et al.*[109] have shown that, for CO_2 electroreduction, decreasing the interparticle spacing for a constant nanoparticle size increases the selectivity for CH_4 and C_2H_4 owing to the increased likelihood of the CO intermediate readsorbing on a neighbouring particle and being further reduced. These phenomena may explain the wide variation in selectivity for Cu nanoparticle catalysts derived from extended, roughened Cu surfaces from highly dispersed Cu nanoparticles on carbon supports.

The nanoparticle shape may also have an important role in the CO_2 reduction reaction, although this parameter has not been much explored. Roberts *et al.*[110] recently investigated Cu nanocubes, grown by successive oxidation–reduction cycles on polycrystalline Cu in the presence of KCl, and found an improvement in C_2H_4 formation. Chen *et al.*[111] synthesized Cu nanocubes using a similar method and also found enhanced C_2H_4 selectivity, as shown in FIG. 4d, and high stability for CO_2 electroreduction. The mechanisms behind the improved activity of these structures may involve the (100) facets on the cubes, which are known to favour C_2H_4 selectivity, the nanostructured Cu cube surface or even Cl^- or Cu^+ species that may remain on the catalyst during the reaction.

Other metal nanoparticles have also shown size dependence in CO_2 electroreduction activity and selectivity[112–114]. For size-controlled Au nanoparticles, it was found that the activity increased significantly below 5 nm in size[113], primarily because of the increase in low-coordinated sites on the nanoparticle surface, as shown in FIG. 5a. Smaller nanoparticles were found to be selective for H_2 owing to weaker COOH* binding on low-coordinated sites under high H* coverage conditions. Similarly, Zhu *et al.*[115,116] studied 4–10-nm Au nanoparticles and nanowires with lengths in the range of

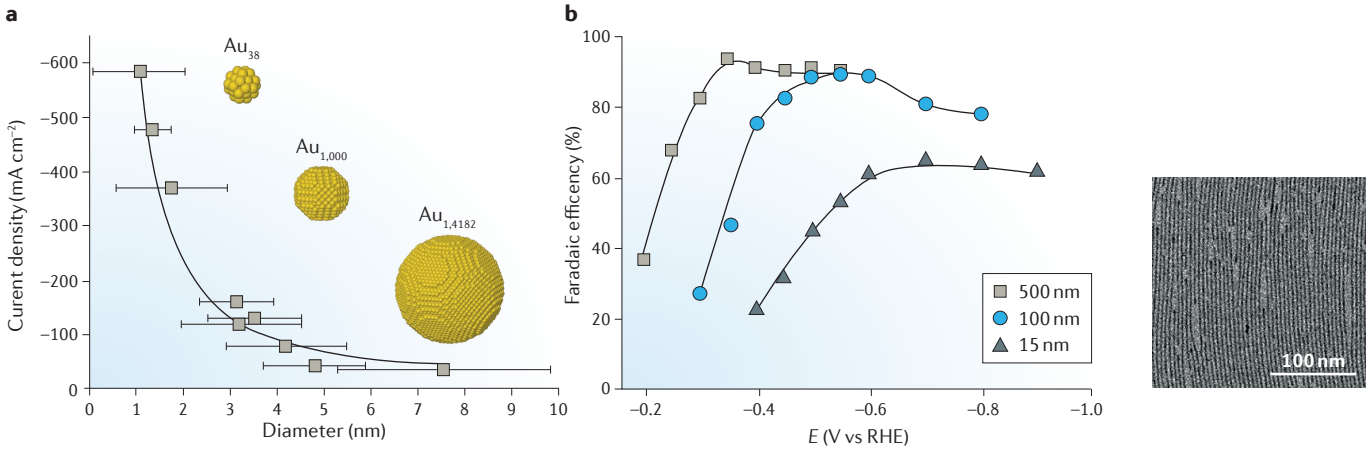

Figure 5 | **Nanostructure effects on activity and selectivity of Au catalysts for CO_2 electroreduction. a** | Nanoparticle size-dependent current density during CO_2 electroreduction over micelle-synthesized Au nanoparticles supported on glassy carbon at −1.2 V versus RHE (reversible hydrogen electrode). **b** | Faradaic efficiency for CO_2 electroreduction to CO for Au nanowires 500, 100 and 15 nm in length supported on carbon. A transmission electron microscope image of the 500 nm-long Au nanowires is also shown. Panel **a** is adapted with permission from REF. 113, American Chemical Society. Panel **b** is adapted with permission from REF. 116, American Chemical Society.

15–500 nm. They reported that larger nanoparticles and longer nanowires were more selective for CO, which they explained in terms of the greater number of edge sites that favour CO_2 reduction compared with corner sites. The Faradaic efficiency of CO production for nanowires of different lengths is shown in FIG. 5b.

A common strategy to improve the catalytic activity of polycrystalline materials is to fabricate rough surfaces with high geometric current densities[117–119]. These rough surfaces can be achieved by dealloying a less noble material from an alloy precursor. Lu *et al.*[120] have used this method to produce a nanoporous Ag catalyst with a large surface area and highly active sites for the reduction of CO_2, which exhibited a 92% Faradaic efficiency of CO production. Other nanoporous materials have also shown high CO_2 reduction efficiency. For example, Cu nanofoams showed improved formate production and suppression of CO, CH_4 and C_2H_4 compared with a smooth polycrystalline Cu foil, probably because of the suppression of the pathway towards the CO* intermediate. Interestingly, these nanofoams showed small Faradaic efficiencies for C_2H_6 and C_3H_6 production[121]. In addition, tuning the composition of porous nanostructured AuCu alloy catalysts resulted in 28% Faradaic efficiency towards methanol and ethanol at a low overpotential[122]. The unique C2, C3 and alcohol selectivity of these catalysts could result from the increased residence time of CO_2 reduction intermediates in the porous structure.

Electronic and geometric structure effects. The formation of metal overlayers offers an attractive opportunity to tune the activity of a given surface[19,123]. The reactivity of metal overlayers is determined by a combination of ligand and strain effects[18,124]. The ligand effect is attributed to a change in the electronic structure caused by the presence of a different atom, whereas the strain effect results from changes in the interatomic distance of the surface atoms when they rearrange to accommodate the substrate. According to the *d*-band model, when the lattice of the surface atoms expands, there is an enhanced interaction with the adsorbates, whereas compression of the lattice has the opposite effect.

In the case of Cu, deposition on a metal, such as Pt or Au, causes expansion of the lattice, leading to a higher binding energy for CO, as shown in FIG. 6a. This change in the reactivity of Cu is expected to have an effect on the catalytic activity, because CO is known to be the key reaction intermediate for hydrocarbon production[91]. To investigate this effect, Januszewska *et al.*[125] prepared differently strained Cu MLs by synthesizing the following multilayer systems on Au(111): 1-ML Cu, 1-ML Cu/1-ML Pd and 1-ML Cu/5-ML Pd. On the basis of only current densities, they observed a clear difference in reduction activity when the Cu overlayer had a different lattice constant, as shown in FIG. 6b, which is evidence that these systems have a different reactivity to pure metals.

Because the activity measured during CO_2 electroreduction can also include the activity for the HER, it is important to analyse the reaction products. Reske *et al.*[126] investigated the effect of Cu overlayer thickness on Pt and found that by increasing the film thickness from 1 ML to 40 MLs, they could enhance the relative Faradaic selectivity for CH_4. They attributed this to modified surface strain, which alters the intermediate binding energies on films of different thickness. Varela *et al.*[127], however, found that 1 ML of Cu on a Pt single crystal was not stable and that, under reaction conditions, the Pt surface was partially exposed owing to the high binding energy between Pt and CO. This observation suggests that the low selectivity for CH_4 observed on 1-ML Cu on Pt does not relate to the Cu–CO binding energy but results from exposed Pt, which favours the HER over CO_2 reduction[127]. These results highlight the importance of taking into account the stability of bimetallic systems under reaction conditions.

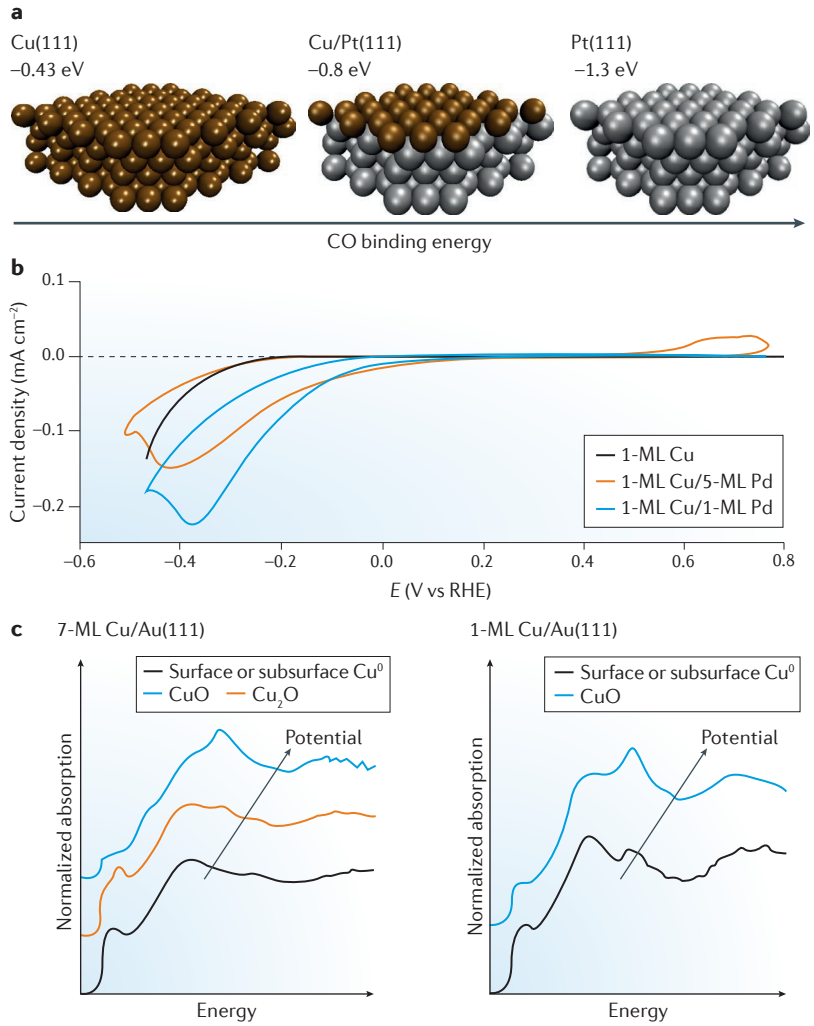

Figure 6 | **Effect of support-induced strain on CO_2 electroreduction catalysts.** **a** | Density functional theory (DFT)-calculated binding energy towards CO on Cu (111), Cu/Pt(111) and Pt(111)[18]. **b** | A single Cu monolayer (ML) deposited on Au(111), or deposited on 1- or 5-ML Pd on Au(111). **c** | High-energy fluorescence-detected X-ray absorption spectra of Cu MLs on Au(111) recorded during the anodic oxidation of Cu in 0.01 M NaOH under $E = 0.31–0.71$ V versus RHE (reversible hydrogen electrode) applied potential (left graph) and $E = 0.11–0.86$ V versus RHE applied potential (right graph). Panel **b** is adapted with permission from REF. 125, American Chemical Society. Panel **c** is adapted with permission from REF. 128, American Chemical Society.

Stability issues may also have a role in Au–Cu systems. Cu MLs on Au(111) have been shown to form islands under applied potential, and Au migration to the surface and alloy formation have been observed[128,129]. Although adsorbates, such as CO and CO_2, do not seem to affect the stability of the Cu ML, at negative potentials Cu forms an interface alloy with the Au atoms, which is probably driven by the interfacial tension between the Cu layer, which is expanded by 12.5%, and the Au (REF. 128). Using high-energy-resolution fluorescence-detected X-ray absorption spectroscopy (HERFD-XAS), Friebel *et al.*[128] have also found that the stability of Cu MLs on Au(111) depends on the number of MLs. Compared with 1-ML Cu/Au(111), 7-ML Cu is resistant to oxidation under an applied potential, which could be related to the incorporation of Cu into the Au surface[128].

The segregation and alloying trends discussed above may be important for understanding the diverse reactivity of AuCu nanoalloy catalysts during CO_2 electroreduction. It has been shown in some studies that selectivity can be tuned from CO to hydrocarbons by changing the composition from Au rich to Cu rich[130,131]. Interestingly, in another study[132], it was shown that even for Cu-rich catalysts, hydrocarbon formation is suppressed in favour of CO formation when Au is added. This phenomenon may be due to the segregation of Au at the catalyst surface owing to its low surface energy or the lowered CO* binding energy in AuCu alloys[133].

Oxide-derived Cu catalysts for hydrocarbon production. Oxide films grown on metal surfaces are commonly used to alter the surface structure of electrodes, and several groups have recently demonstrated an enhanced activity of oxide-derived nanostructured Cu for CO_2 electroreduction after an assumed *in situ* reduction in the electrochemical environment. Although CH_4 is the dominant hydrocarbon product formed on bulk metallic Cu, almost complete CH_4 suppression has been reported on oxide-derived, electrochemically reduced Cu catalysts, along with improved efficiency for C_2H_4 and C_2H_6 and a shift to a lower CO_2 reduction overpotential[117,134–136]. These results are likely attributed to pH, morphological effects and possible changes of the chemical state of the active Cu species. The synthesis and reduction of these oxide films strongly affect the surface structure, which may be a determining factor in the resulting behaviour of the catalysts.

The initial oxide film thickness also appears to have a key role in determining the selectivity of oxide-derived Cu. Koper and colleagues[135] found that by increasing the initial oxide film thickness, the C_2H_4 selectivity diminished, whereas C_2H_6 selectivity was improved. Interestingly, Yeo and colleagues[136] found a parabolic dependence of the selectivity for C_2H_4 on the initial oxide film thickness between 0.2 and 8.8 µm, with intermediate film thicknesses showing the highest C_2H_4 selectivity of approximately 40%. In both cases, CH_4 selectivity was suppressed with increasing oxide thickness. These results are likely to be attributable to pH and morphological effects.

Kanan and colleagues[117] synthesized oxide-derived Cu through thermal annealing and reported a high Faradaic efficiency (~45%) for CO_2 conversion at potentials as low as −0.3 V versus RHE (reversible hydrogen electrode), although limited hydrocarbon production was observed at higher potentials. They later suggested that grain boundaries may stabilize strong CO-binding sites on oxide-derived catalysts, thereby enabling the efficient reduction of CO to hydrocarbons[137,138].

It is generally assumed that the active species for CO_2 electroreduction is metallic Cu and that oxide-derived catalysts are completely reduced during the reaction. However, a possible mechanism behind the unique reactivity of oxide-derived Cu may involve Cu^+ sites that remain on the surface. Kim *et al.*[134] proposed that oxide species remain on the Cu catalyst surface during the reaction, as determined from *ex situ* Auger measurements.

It has been proposed that Cu_2O might be the active species for methanol production[139,140], although few groups have demonstrated notable methanol formation through electrochemical CO_2 reduction because of the instability of oxides during the reaction[141]. The use of ZnO as a support for Cu catalysts increases the selectivity for alcohols, possibly by stabilizing low-coordinated active sites or Cu^+ species on Cu, or through ligand effects[142]. These results reveal interesting analogies between the electrocatalytic and the conventional (thermal) catalytic reaction pathway from CO_2 to methanol, which is known to be catalysed by Cu/ZnO active sites[143]. In summary, although oxide-derived Cu catalysts are the most promising in terms of CO_2 reduction efficiency, key questions remain about the fundamental mechanism behind this improvement. *In situ* and *operando* studies, instead of *ex situ* prenatal or post-mortem studies, which currently provide the majority of available characterization data for this reaction, are essential to solve these questions and ultimately gain an insight into the chemical state of the active catalyst under reaction conditions.

Effect of electrolyte and pH on selectivity. For nanostructured catalysts, the electrolyte can have a key role in controlling the selectivity of the reaction[144,145]. For CO_2 reduction over Cu, the selectivity between CH_4 or C_2H_4 can be considerably altered in different electrolytes[146]. Such changes can be attributed to the different nature of the ions in solution. For example, cationic species (Li^+, Na^+, K^+ and Cs^+) in bicarbonate solutions can be used to control the CH_4/C_2H_4 ratio[147].

CO_2 reduction is usually carried out in bicarbonate electrolytes at a close-to-neutral pH, because CO_2 acts as a buffer. Considering the challenges of working at different pH values in CO_2-saturated electrolytes, studies on the effect of bulk pH have focused on the reduction of CO at different pH values[148–150]. For CO reduction at a pH between 6 and 12, the formation of CH_4 is pH dependent[148], which indicates that this process occurs via coupled proton–electron transfer[151]. By contrast, C_2H_4 formation is independent of pH; thus, this process is not determined by the concentration. As a result, C_2H_4 is the predominant hydrocarbon product under alkaline conditions, whereas in acidic or neutral solutions CH_4 formation is preferred[148]. This knowledge is relevant when working under neutral conditions, as is common for CO_2 reduction, in which small changes in local proton concentration can have a dramatic effect on the interfacial pH, which affects the reaction selectivity. Gupta *et al.*[152] estimated, on the basis of a theoretical study, the local pH during CO_2 electroreduction and found that it can be up to six units higher than the bulk pH, depending on the thickness of the diffusion layer, the current density and the electrolyte buffer capacity. This last parameter can be related to the concentration of bicarbonate, because concentrated carbonate electrolytes possess an enhanced capability to suppress local pH increases during the catalytic consumption of interfacial protons.

The selectivity of Cu is dependent on the bicarbonate concentration. Dilute $KHCO_3$ electrolytes with an alkaline pH result in high selectivity for C_2H_4. By contrast, when the concentration of bicarbonate is high, the local pH remains close to neutral, favouring CH_4 and H_2 production[135,145,146]. Varela *et al.*[145] have recently shown that the change in selectivity occurs mainly because of a suppression of CH_4 production in electrolytes with a low buffering capacity. Under such conditions, the low proton concentration near the interface affects the proton-dependent reactions (that is, the HER and CH_4 production), whereas the production rate of C_2H_4 is not affected.

According to Gupta's model[152], the current is also an important parameter. High current densities correspond to a higher consumption of interfacial protons and, therefore, to more dramatic changes in local pH. In general, the geometric current densities are higher on rough surfaces at a given electrode potential than on smooth surfaces. If the diffusion layer is sufficiently thick, this can result in a higher local interfacial pH at the rough catalyst surface, which, in turn, inhibits H_2 and CH_4 formation in favour of C_2H_4 (REFS 110,117,118,135).

Considering the key role that the local pH has in controlling the selectivity of CO_2 conversion over Cu for CH_4 and C_2H_4, critical investigation of the interplay among the pH, catalyst structure and morphology is necessary.

Ethanol oxidation

Ethanol electrooxidation is a promising reaction for energy production in fuel cells, but similar to CO_2 reduction, it is currently hindered by the poor selectivity exhibited in common electrocatalyst materials. Instead of complete oxidation to CO_2, which requires the breaking of the C–C bond either in ethanol or the acetaldehyde intermediate, many catalysts produce only acetaldehyde and acetic acid, the latter of which cannot be further oxidized to CO_2. In addition, ethanol oxidation catalysts commonly have a high Pt content, making them expensive and unfeasible to scale up. Furthermore, the poisoning of active sites by strongly adsorbed CO and CH_x intermediate species can hinder the activity of Pt catalysts for this reaction. As we detail in this section, the results from recent studies of structure-dependent selectivity in ethanol oxidation suggest that nanostructured and bimetallic materials may be the key to optimizing the selectivity for CO_2.

Structure-dependent selectivity on single crystals. The structure dependence of the ethanol oxidation reaction is evident from studies of single-crystal Pt electrodes. When comparing the different crystallographic surfaces of Pt in acidic media, (111) surfaces were found to be inefficient at breaking C–C bonds, whereas (110) surfaces had the highest rate of C–C bond cleavage[153]. However, it has become clear from studies of stepped surfaces that efficient C–C bond cleavage is not the only necessary characteristic for a good ethanol total oxidation catalyst[154]. In addition, sufficient coverage of adsorbed OH species is necessary. Colmati *et al.*[155] found that Pt(554) surfaces have the optimal number of (110) steps, which can break C–C bonds at an intermediate rate such that the CO formed will not poison the surface but will be further oxidized by OH species. As Lai *et al.*[156]

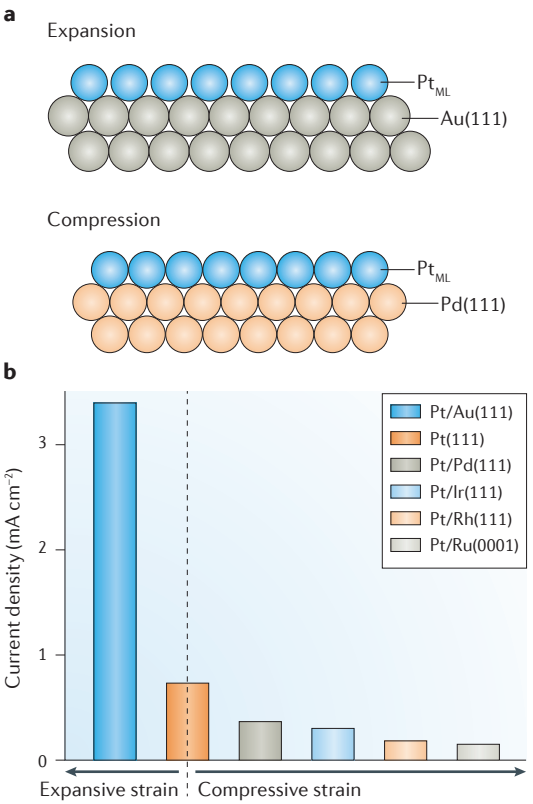

Figure 7 | **Strain-induced enhancement in the catalytic activity of Pt MLs for ethanol oxidation. a** | Models illustrating an epitaxial Pt monolayer (ML) on Au(111), which induces expansive strain on the Pt, and a Pt ML on Pd(111), which exerts compressive strain. **b** | Current density towards ethanol oxidation on Pt MLs deposited on different single crystals. Adapted with permission from REF. 172, American Chemical Society.

have shown, it is important to consider the effect of strongly adsorbing ions in the electrolyte that can alter the activity and selectivity trends on stepped surfaces. To achieve the balance between efficient C–C bond cleavage (which leads to surface poisoning by adsorbed CO) and sufficient adsorption of OH (which oxidizes the CO), the addition of a second metal, such as Ru, can stabilize the adsorbed OH (REF. 157). This mechanism is important in alloy catalysts, as we discuss below. In alkaline media, higher current densities for ethanol oxidation can be achieved at potentials more relevant for fuel cells. The reaction is highly dependent on the Pt surface structure; however, fast deactivation can occur on Pt(111) terraces owing to poor oxidation of CH_x species on the surface[158].

From the studies on model surfaces discussed above, it is clear that structure has a strong effect on ethanol oxidation reactivity, although the effects of nanoparticle size and shape on ethanol electrooxidation have not been widely explored. One notable example, however, is the work of Sun and colleagues[159,160] on Pt and Pd nanocrystals with stable high-index facets. High-index facets on tetrahexahedral Pt nanoparticles show higher activity and selectivity for CO_2 than commercial Pt/C catalysts because of the ability of atomic steps to cleave C–C bonds[159,160]. Furthermore, they found a four- to six-fold improvement in activity for similar tetrahexahedral Pd nanoparticles with high-index facets compared with commercial Pd/C (REF. 161).

Although interesting insights into the reaction mechanism have been derived from studies of single crystals and well-defined particles, more complex alloy catalysts are needed to achieve sufficiently low overpotentials for efficient fuel cell operation.

Bimetallic nanostructures. Alloying Pt with other metals to create binary or ternary catalysts is a well-established strategy to enhance the catalytic performance for ethanol electrooxidation[162]. Although a range of binary and ternary nanocatalysts are being explored for this reaction, we focus on studies of model catalysts that have involved various measurement techniques to elucidate the mechanism behind the activity and selectivity of these materials.

As explained above, one of the main challenges with Pt ethanol oxidation catalysts is poisoning of the surface by the accumulation of adsorbed CO. Alloying with Sn can improve the activity of Pt via a dual mechanism whereby Sn stabilizes OH, which can further oxidize CO (REF. 163). The structure and oxidation state of these catalysts are also important because SnO_2 enhances C–C cleavage, unlike alloyed Sn (REF. 164). Alternatively, the activity of Pt-alloy catalysts can be considerably enhanced by replacing the Sn component with Ni, which has a superior O-donating effect[165].

The Pt–Rh–Sn system is one of the most promising ternary catalysts studied for ethanol electrooxidation, because it can catalyse total ethanol oxidation with high efficiency at potentials below 0.5 V versus RHE[166–171]. It was recently shown that $PtRhSnO_2$/C catalysts have high activity and selectivity for CO_2 owing to the electronic interactions between the metals; because Pt withdraws electrons from Rh, the interaction between Rh and ethanol becomes strong enough to break the C–C bond. Conversely, SnO_2 contributes to the catalytic performance by strongly adsorbing H_2O, thereby minimizing the formation of activity-blocking PtOH and RhOH (REF. 167). The structure of the Pt–Rh–Sn system may be crucial for its activity, because specific active-site ensembles may be necessary to facilitate the reaction[166]. The addition of Ir to Pt–SnO_2 catalysts can also cleave C–C bonds and lower the overpotential of ethanol oxidation[171].

Another mechanism that may affect bimetallic ethanol oxidation catalysts involves geometric effects due to lattice-mismatch-induced strain. This has a major impact on the activity of epitaxial Pt MLs on various single crystals. Surfaces such as Au(111), which exert tensile strain on Pt, are more active for ethanol and methanol oxidation; however, these surfaces are only selective for the partial oxidation products acetaldehyde and acetic acid[172]. By contrast, surfaces that induce compressive strain on the Pt ML, such as Pd(111), Ir(111), Rh(111) and Ru(0001), suppress ethanol oxidation activity. A summary of these observations is provided in FIG. 7. Pt MLs deposited on Au nanoparticles, tested for ethanol electrooxidation by Loukrakpam *et al.*[173], were

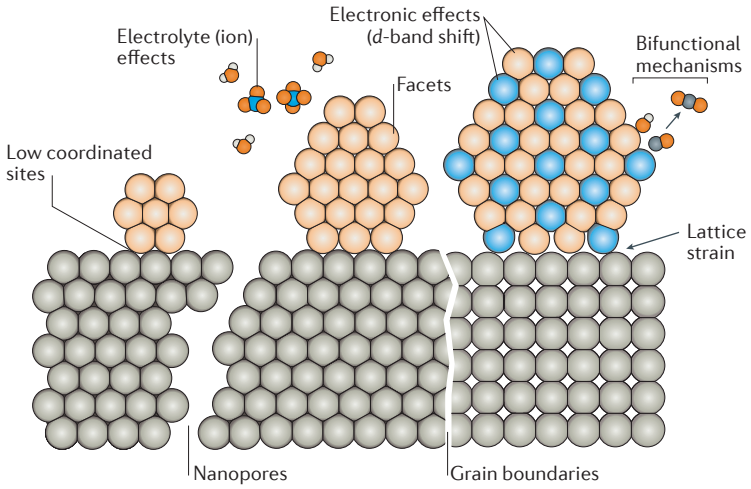

Figure 8 | **Overview of the mechanisms behind activity and selectivity control in nanostructured electrocatalysts.** Structural features, such as low-coordinated sites, facets, nanopores and grain boundaries, can be tuned to control reactivity. In bimetallic nanostructures, strain effects, electronic effects and bifunctional effects can be tuned. In addition, reactivity trends may be strongly influenced by environmental factors such as the properties of the electrolyte and pH.

found to have higher activity and higher efficiency for CO_2 reduction than Pt sub-ML/Au nanoparticles. This result was rationalized in terms of these catalysts having the optimal balance between tensile strain induced by lattice mismatch with the Au support and compressive strain induced by finite-size effects. In summary, ethanol electrooxidation is highly sensitive to the structure and composition of nanocatalysts.

Summary and outlook

We have demonstrated how rational control over the structure and composition of metallic nanocatalysts can be used to tune activity and selectivity for O_2 reduction, CO_2 reduction and ethanol oxidation, which are key reactions for emerging electrochemical energy conversion and storage processes. The main mechanisms behind the improved activity and selectivity in the nano-electrocatalysts discussed are summarized in FIG. 8. In terms of structure, morphology-controlled nanostructures may have the optimal particle size and/or shape to provide highly active, low-coordinated sites, such as corners and edges, or optimal facets that can facilitate a reaction step. Defects, such as grain boundaries, may also stabilize active sites. The interparticle distance is another crucial but often overlooked parameter that can be used to control the diffusion and readsorption of reaction intermediates and, therefore, the selectivity. Nanopores also provide low-coordinated sites for a reaction and can alter the selectivity by increasing the residence time of intermediates. For multimetallic catalysts, further mechanisms may contribute, such as geometric and ligand effects. Finally, in an electrochemical reaction, it is important to consider the effects of the electrolyte and ions in the solution, which may strongly adsorb on the catalyst surface, react with the surface to alter the structure or change the pH.

To develop feasible renewable energy technology based on fuel cells and to close the carbon cycle through CO_2 conversion, several key challenges in electrocatalyst design must be overcome. From the studies highlighted in this Review, it is clear that novel synthesis methods that allow for the design of model catalysts with control over the morphology, structure, chemical state and composition have enabled outstanding advances in the field of electrocatalysis. However, these synthesis methods must be scalable, and, particularly for the ORR and ethanol oxidation, new catalyst materials that are cheaper and more durable, or that can at least minimize the use of expensive Pt-group metals, must be developed. Another challenge is to better engineer selectivity for a single product to avoid separation costs, which is important for CO_2 conversion and for ethanol oxidation.

The nature of these catalysts is highly complex — the nanostructure and active chemical species of the catalyst can be not only used to control the reaction but also changed during the reaction or by environmental factors such as the temperature and the properties of the electrolyte. Therefore, it is necessary to use *in situ* and *in operando* techniques to monitor the catalyst properties during the reaction to gain a complete understanding of the reaction mechanism. These techniques, combined with theoretical modelling, can provide an insight into the working structural and chemical states of the most active catalysts and provide the basic understanding needed to rationally design and tailor the properties of new catalysts.

1. Vielstich, W., Lamm, A. & Gasteiger, H. *Handbook of Fuel Cells — Fundamentals, Technology, and Applications* (Wiley, 2003).
2. Gasteiger, H. A., Kocha, S. S., Sompalli, B. & Wagner, F. T. Activity benchmarks and requirements for Pt, Pt-alloy, and non-Pt oxygen reduction catalysts for PEMFCs. *Appl. Catal. B* **56**, 9–35 (2005).
3. Debe, M. K. Electrocatalyst approaches and challenges for automotive fuel cells. *Nature* **486**, 43–51 (2012).
4. Evans, U. R. Cathodic reduction of oxygen in fuel cells and corrosion cells. *Nature* **218**, 602–603 (1968).
5. Liang, C. C. & Juliard, A. L. Reduction of oxygen at platinum electrode. *Nature* **207**, 629–630 (1965).
6. Huang, X. *et al.* High-performance transition metal-doped Pt_3Ni octahedra for oxygen reduction reaction. *Science* **348**, 1230–1234 (2015).
7. Marković, N. M. & Ross, P. N. Surface science studies of model fuel cell electrocatalysts. *Surf. Sci. Rep.* **45**, 117–229 (2002).
8. Jiao, Y., Zheng, Y., Jaroniec, M. T. & Qiao, S. Z. Design of electrocatalysts for oxygen- and hydrogen-involving energy conversion reactions. *Chem. Soc. Rev.* **44**, 2060–2086 (2015).
9. Nie, Y., Li, L. & Wei, Z. D. Recent advancements in Pt and Pt-free catalysts for oxygen reduction reaction. *Chem. Soc. Rev.* **44**, 2168–2201 (2015).
10. Stephens, I. E. L., Bondarenko, A. S., Andersen, U. G., Rossmeisl, J. & Chorkendorff, I. Understanding the electrocatalysis of oxygen reduction on platinum and its alloys. *Energy Environ. Sci.* **5**, 6744–6762 (2012).
11. Bing, Y., Liu, H., Zhang, L., Ghosh, D. & Zhang, J. Nanostructured Pt-alloy electrocatalysts for PEM fuel cell oxygen reduction reaction. *Chem. Soc. Rev.* **39**, 2184–2202 (2010).
12. Krischer, K. & Savinova, E. R. in *Handbook of Heterogeneous Catalysis* (eds Ertl, G., Knözinger, H. & Weitkamp, J.) 1873–1905 (Wiley, 2008).
13. Markovic, N., Schmidt, T., Stamenkovic, V. & Ross, P. Oxygen reduction reaction on Pt and Pt bimetallic surfaces: a selective review. *Fuel Cells* **1**, 105–116 (2001).
14. Nørskov, J. K. *et al.* Origin of the overpotential for oxygen reduction at a fuel-cell cathode. *J. Phys. Chem. B* **108**, 17886–17892 (2004).
15. Abild-Pedersen, F. *et al.* Scaling properties of adsorption energies for hydrogen-containing molecules on transition-metal surfaces. *Phys. Rev. Lett.* **99**, 016105 (2007).
16. Stephens, I. E. L. *et al.* Tuning the activity of Pt(111) for oxygen electroreduction by subsurface alloying. *J. Am. Chem. Soc.* **133**, 5485–5491 (2011).
17. Adžić, R., Strbac, S. & Anastasijević, N. Electrocatalysis of oxygen on single crystal gold electrodes. *Mater. Chem. Phys.* **22**, 349–375 (1989).
18. Mavrikakis, M., Hammer, B. & Nørskov, J. K. Effect of strain on the reactivity of metal surfaces. *Phys. Rev. Lett.* **81**, 2819 (1998).
19. Kibler, L. A., El-Aziz, A. M., Hoyer, R. & Kolb, D. M. Tuning reaction rates by lateral strain in a palladium monolayer. *Angew. Chem. Int. Ed. Engl.* **44**, 2080–2084 (2005).

20. Zhang, J., Vukmirovic, M. B., Xu, Y., Mavrikakis, M. & Adzic, R. R. Controlling the catalytic activity of platinum-monolayer electrocatalysts for oxygen reduction with different substrates. *Angew. Chem. Int. Ed. Engl.* **44**, 2132–2135 (2005).
21. Genorio, B. *et al.* Tailoring the selectivity and stability of chemically modified platinum nanocatalysts to design highly durable anodes for PEM fuel cells. *Angew. Chem. Int. Ed. Engl.* **50**, 5468–5472 (2011).
22. Genorio, B. *et al.* Selective catalysts for the hydrogen oxidation and oxygen reduction reactions by patterning of platinum with calix[4]arene molecules. *Nat. Mater.* **9**, 998–1003 (2010).
23. Kinoshita, K. Particle size effects for oxygen reduction on highly dispersed platinum in acid electrolytes. *J. Electrochem. Soc.* **137**, 845–848 (1990).
24. Mukerjee, S. Particle size and structural effects in platinum electrocatalysis. *J. Appl. Electrochem.* **20**, 537–548 (1990).
25. Mukerjee, S. & McBreen, J. Effect of particle size on the electrocatalysis by carbon-supported Pt electrocatalysts: an *in situ* XAS investigation. *J. Electroanal. Chem.* **448**, 163–171 (1998).
26. Kuzume, A., Herrero, E. & Feliu, J. M. Oxygen reduction on stepped platinum surfaces in acidic media. *J. Electroanal. Chem.* **599**, 333–343 (2007).
27. Markovic, N. M., Gasteiger, H. A. & Ross, P. N. Oxygen reduction on platinum low-index single-crystal surfaces in alkaline solution: rotating ring $disk_{Pt(hkl)}$ studies. *J. Phys. Chem.* **100**, 6715–6721 (1996).
28. Bandarenka, A. S., Hansen, H. A., Rossmeisl, J. & Stephens, I. E. L. Elucidating the activity of stepped Pt single crystals for oxygen reduction. *Phys. Chem. Chem. Phys.* **16**, 13625–13629 (2014).
29. Mayrhofer, K. *et al.* The impact of geometric and surface electronic properties of Pt catalysts on the particle size effect in electrocatalysis. *J. Phys. Chem. B* **109**, 14433–14440 (2005).
30. Shao, M., Peles, A. & Shoemaker, K. Electrocatalysis on platinum nanoparticles: particle size effect on oxygen reduction reaction activity. *Nano Lett.* **11**, 3714–3719 (2011).
31. Perez-Alonso, F. J. *et al.* The effect of size on the oxygen electroreduction activity of mass-selected platinum nanoparticles. *Angew. Chem. Int. Ed. Engl.* **51**, 4641–4643 (2012).
32. Takasu, Y. *et al.* Size effects of platinum particles on the electroreduction of oxygen. *Electrochim. Acta* **41**, 2595–2600 (1996).
33. Gara, M., Ward, K. & Compton, R. Nanomaterial modified electrodes: evaluating oxygen reduction catalysts. *Nanoscale* **5**, 7304–7311 (2013).
34. Schneider, A. *et al.* Transport effects in the oxygen reduction reaction on nanostructured, planar glassy carbon supported Pt/GC model electrodes. *Phys. Chem. Chem. Phys.* **10**, 1931–1943 (2008).
35. Seidel, Y. *et al.* Mesoscopic mass transport effects in electrocatalytic processes. *Faraday Discuss.* **140**, 167–184 (2009).
36. Kumar, S. & Zou, S. Electroreduction of O_2 on uniform arrays of Pt and PtCo nanoparticles. *Electrochem. Commun.* **8**, 1151–1157 (2006).
37. Yang, H., Kumar, S. & Zou, S. Electroreduction of O_2 on uniform arrays of Pt nanoparticles. *J. Electroanal. Chem.* **688**, 180–188 (2013).
38. Speder, J. *et al.* The particle proximity effect: from model to high surface area fuel cell catalysts. *RSC Adv.* **4**, 14971–14978 (2014).
39. Nesselberger, M. *et al.* The effect of particle proximity on the oxygen reduction rate of size-selected platinum clusters. *Nat. Mater.* **12**, 919–924 (2013).
40. Thompsett, D. in *Handbook of Fuel Cells: Fundamentals Technology and Applications* Vol. 3 Ch. 37 (eds Vielstich, W., Lamm, A. & Gasteiger, H.) 467 (Wiley, 2003).
41. Strasser, P. Catalysts by platonic design. *Science* **349**, 379–380 (2015).
42. Carpenter, M. K., Moylan, T. E., Kukreja, R. S., Atwan, M. H. & Tessema, M. M. Solvothermal synthesis of platinum alloy nanoparticles for oxygen reduction electrocatalysis. *J. Am. Chem. Soc.* **134**, 8535–8542 (2012).
43. Cui, C. *et al.* Octahedral PtNi nanoparticle catalysts: exceptional oxygen reduction activity by tuning the alloy particle surface composition. *Nano Lett.* **12**, 5885–5889 (2012).
44. Gan, L. *et al.* Element-specific anisotropic growth of shaped platinum alloy nanocrystals. *Science* **346**, 1502–1506 (2014).
45. Wu, J. B. *et al.* Truncated octahedral Pt_3Ni oxygen reduction reaction electrocatalysts. *J. Am. Chem. Soc.* **132**, 4984–4985 (2010).
46. Choi, S.-I. *et al.* Synthesis and characterization of 9 nm Pt–Ni octahedra with a record high activity of 3.3 A/mg_{Pt} for the oxygen reduction reaction. *Nano Lett.* **13**, 3420–3425 (2013).
47. Zhang, J., Yang, H., Fang, J. & Zou, S. Synthesis and oxygen reduction activity of shape-controlled Pt_3Ni nanopolyhedra. *Nano Lett.* **10**, 638–644 (2010).
48. Cui, C. *et al.* Shape-selected bimetallic nanoparticle electrocatalysts: evolution of their atomic-scale structure, chemical composition, and electrochemical reactivity under various chemical environments. *Faraday Discuss.* **162**, 91–112 (2013).
49. Cui, C., Gan, L., Heggen, M., Rudi, S. & Strasser, P. Compositional segregation in shaped Pt alloy nanoparticles and their structural behaviour during electrocatalysis. *Nat. Mater.* **12**, 765–771 (2013).
50. Cui, C. *et al.* Carbon monoxide-assisted size confinement of bimetallic alloy nanoparticles. *J. Am. Chem. Soc.* **136**, 4813–4816 (2014).
51. Paulus, U. *et al.* Oxygen reduction on high surface area Pt-based alloy catalysts in comparison to well defined smooth bulk alloy electrodes. *Electrochim. Acta* **47**, 3787–3798 (2002).
52. Paulus, U. *et al.* Oxygen reduction on carbon-supported Pt–Ni and Pt–Co alloy catalysts. *J. Phys. Chem. B* **106**, 4181–4191 (2002).
53. Stamenkovic, V., Schmidt, T., Ross, P. & Markovic, N. Surface composition effects in electrocatalysis: kinetics of oxygen reduction on well-defined Pt_3Ni and Pt_3Co alloy surfaces. *J. Phys. Chem. B* **106**, 11970–11979 (2002).
54. Anderson, A. B. *et al.* Activation energies for oxygen reduction on platinum alloys: theory and experiment. *J. Phys. Chem. B* **109**, 1198–1203 (2005).
55. Stamenkovic, V. *et al.* Changing the activity of electrocatalysts for oxygen reduction by tuning the surface electronic structure. *Angew. Chem. Int. Ed. Engl.* **118**, 2963–2967 (2006).
56. Stamenkovic, V. R. *et al.* Improved oxygen reduction activity on $Pt_3Ni(111)$ via increased surface site availability. *Science* **315**, 493–497 (2007).
57. Stamenkovic, V. R. *et al.* Trends in electrocatalysis on extended and nanoscale Pt-bimetallic alloy surfaces. *Nat. Mater.* **6**, 241–247 (2007).
58. Wang, C. *et al.* Monodisperse Pt_3Co nanoparticles as a catalyst for the oxygen reduction reaction: size-dependent activity. *J. Phys. Chem. C* **113**, 19365–19368 (2009).
59. Wang, C. *et al.* Multimetallic Au/$FePt_3$ nanoparticles as highly durable electrocatalyst. *Nano Lett.* **11**, 919–926 (2010).
60. van der Vliet, D. F. *et al.* Unique electrochemical adsorption properties of Pt-skin surfaces. *Angew. Chem. Int. Ed. Engl.* **124**, 3193–3196 (2012).
61. Wang, C. *et al.* Rational development of ternary alloy electrocatalysts. *J. Phys. Chem. Lett.* **3**, 1668–1673 (2012).
62. Wang, C., Markovic, N. M. & Stamenkovic, V. R. Advanced platinum alloy electrocatalysts for the oxygen reduction reaction. *ACS Catal.* **2**, 891–898 (2012).
63. Chen, C. *et al.* Highly crystalline multimetallic nanoframes with three-dimensional electrocatalytic surfaces. *Science* **343**, 1339–1343 (2014).
64. Zhang, J. *et al.* Mixed-metal Pt monolayer electrocatalysts for enhanced oxygen reduction kinetics. *J. Am. Chem. Soc.* **127**, 12480–12481 (2005).
65. Nilekar, A. U. *et al.* Bimetallic and ternary alloys for improved oxygen reduction catalysis. *Top. Catal.* **46**, 276–284 (2007).
66. Wang, J. X. *et al.* Oxygen reduction on well-defined core–shell nanocatalysts: particle size, facet, and Pt shell thickness effects. *J. Am. Chem. Soc.* **131**, 17298–17302 (2009).
67. Sasaki, K. *et al.* Core-protected platinum monolayer shell high-stability electrocatalysts for fuel-cell cathodes. *Angew. Chem. Int. Ed. Engl.* **49**, 8602–8607 (2010).
68. Karan, H. I. *et al.* Catalytic activity of platinum monolayer on iridium and rhenium alloy nanoparticles for the oxygen reduction reaction. *ACS Catal.* **2**, 817–824 (2012).
69. Sasaki, K. *et al.* Highly stable Pt monolayer on PdAu nanoparticle electrocatalysts for the oxygen reduction reaction. *Nat. Commun.* **3**, 1115 (2012).
70. Zhang, Y. *et al.* Hollow core supported Pt monolayer catalysts for oxygen reduction. *Catal. Today* **202**, 50–54 (2013).
71. Koh, S. & Strasser, P. Electrocatalysis on bimetallic surfaces: modifying catalytic reactivity for oxygen reduction by voltammetric surface dealloying. *J. Am. Chem. Soc.* **129**, 12624–12625 (2007).
72. Mani, P. Srivastava, R. & Strasser, P. Dealloyed Pt–Cu core–shell nanoparticle electrocatalysts for use in PEM fuel cell cathodes. *J. Phys. Chem. C* **112**, 2770–2778 (2008).
73. Strasser, P. in *Handbook of Fuel Cells: Advances in Electrocatalysis, Materials, Diagnostics and Durability* (eds Lamm, A., Vielstich, W., Yokokawa, H. & Gasteiger, H. A.) 30–47 (Wiley, 2010).
74. Strasser, P. Dealloyed core–shell fuel cell electrocatalysts. *Rev. Chem. Eng.* **25**, 255–295 (2009).
75. Strasser, P. *et al.* Lattice-strain control of the activity in dealloyed core–shell fuel cell catalysts. *Nat. Chem.* **2**, 454–460 (2010).
76. Gan, L., Heggen, M., O'Malley, R., Theobald, B. & Strasser, P. Understanding and controlling nanoporosity formation for improving the stability of bimetallic fuel cell catalysts. *Nano Lett.* **13**, 1131–1138 (2013).
77. Oezaslan, M., Hasché, F.d.r. & Strasser, P. Pt-based core–shell catalyst architectures for oxygen fuel cell electrodes. *J. Phys. Chem. Lett.* **4**, 3273–3291 (2013).
78. Gan, L., Heggen, M., Rudi, S. & Strasser, P. Core–shell compositional fine structures of dealloyed Pt_xNi_{1-x} nanoparticles and their impact on oxygen reduction catalysis. *Nano Lett.* **12**, 5423–5430 (2012).
79. Han, B. *et al.* Record activity and stability of dealloyed bimetallic catalysts for proton exchange membrane fuel cells. *Energy Environ. Sci.* **8**, 258–266 (2015).
This study reported the most active and stable performance of a size-controlled dealloyed $PtNi_3$ core–shell nanoparticle catalyst during a realistic PEM fuel cell test.
80. Neyerlin, K. C. Srivastava, R., Yu, C. & Strasser, P. Electrochemical activity and stability of dealloyed Pt–Cu and Pt–Cu–Co electrocatalysts for the oxygen reduction reaction (ORR). *J. Power Sources* **186**, 261–267 (2009).
81. Wu, J. B., Gross, A. & Yang, H. Shape and composition-controlled platinum alloy nanocrystals using carbon monoxide as reducing agent. *Nano Lett.* **11**, 798–802 (2011).
82. Wu, J. *et al.* Icosahedral platinum alloy nanocrystals with enhanced electrocatalytic activities. *J. Am. Chem. Soc.* **134**, 11880–11883 (2012).
83. Kondratenko, E. V., Mul, G., Baltrusaitis, J., Larrazábal, G. O. & Pérez-Ramírez, J. Status and perspectives of CO_2 conversion into fuels and chemicals by catalytic, photocatalytic and electrocatalytic processes. *Energy Environ. Sci.* **6**, 3112–3135 (2013).
84. Hori, Y. in *Modern Aspects of Electrochemistry* (eds Vayenas, C. G., White, R. E. & Gamboa-Aldeco, M. E.) 89–189 (Springer, 2008).
85. Costentin, C., Robert, M. & Savéant, J.-M. Catalysis of the electrochemical reduction of carbon dioxide. *Chem. Soc. Rev.* **42**, 2423–2436 (2013).
86. Asadi, M. *et al.* Robust carbon dioxide reduction on molybdenum disulphide edges. *Nat. Commun.* **5**, 4470 (2014).
87. Kuhl, K. P., Cave, E. R., Abram, D. N. & Jaramillo, T. F. New insights into the electrochemical reduction of carbon dioxide on metallic copper surfaces. *Energy Environ. Sci.* **5**, 7050–7059 (2012).
88. Kuhl, K. P. *et al.* Electrocatalytic conversion of carbon dioxide to methane and methanol on transition metal surfaces. *J. Am. Chem. Soc.* **136**, 14107–14113 (2014).
89. Varela, A. S. *et al.* Metal-doped nitrogenated carbon as efficient catalyst for direct CO_2 electroreduction to CO and hydrocarbons. *Angew. Chem. Int. Ed. Engl.* **54**, 10758–10762 (2015).
90. Peterson, A. A. & Nørskov, J. K. Activity descriptors for CO_2 electroreduction to methane on transition-metal catalysts. *J. Phys. Chem. Lett.* **3**, 251–258 (2012).
91. Peterson, A. A., Abild-Pedersen, F., Studt, F., Rossmeisl, J. & Nørskov, J. K. How copper catalyzes the electroreduction of carbon dioxide into hydrocarbon fuels. *Energy Environ. Sci.* **3**, 1311–1315 (2010).
92. Shi, C., Hansen, H. A., Lausche, A. C. & Nørskov, J. K. Trends in electrochemical CO_2 reduction activity for open and close-packed metal surfaces. *Phys. Chem. Chem. Phys.* **16**, 4720–4727 (2014).

93. Hansen, H. A., Varley, J. B., Peterson, A. A. & Nørskov, Understanding, J. K. Trends in the electrocatalytic activity of metals and enzymes for CO_2 reduction to CO. *J. Phys. Chem. Lett.* **4**, 388–392 (2013).
94. Akhade, S. A. *et al.* Poisoning effect of adsorbed CO during CO_2 electroreduction on late transition metals. *Phys. Chem. Chem. Phys.* **16**, 20429–20435 (2014).
95. Hori, Y., Takahashi, I., Koga, O. & Hoshi, N. Selective formation of C2 compounds from electrochemical reduction of CO_2 at a series of copper single crystal electrodes. *J. Phys. Chem. B* **106**, 15–17 (2002).
96. Durand, W. J., Peterson, A. A., Studt, F., Abild-Pedersen, F. & Nørskov, J. K. Structure effects on the energetics of the electrochemical reduction of CO_2 by copper surfaces. *Surf. Sci.* **605**, 1354–1359 (2011).
97. Schouten, K. J. P., Qin, Z., Gallent, E. P. & Koper, M. T. Two pathways for the formation of ethylene in CO reduction on single-crystal copper electrodes. *J. Am. Chem. Soc.* **134**, 9864–9867 (2012).
98. Schouten, K., Kwon, Y., Van der Ham, C., Qin, Z. & Koper, M. T. A new mechanism for the selectivity to C1 and C2 species in the electrochemical reduction of carbon dioxide on copper electrodes. *Chem. Sci.* **2**, 1902–1909 (2011).
99. Montoya, J. H., Shi, C., Chan, K. & Norskov, J. K. Theoretical insights into a CO dimerization mechanism in CO_2 electroreduction. *J. Phys. Chem. Lett.* **6**, 2032–2037 (2015).
100. Nie, X., Esopi, M. R., Janik, M. J. & Asthagiri, A. Selectivity of CO_2 reduction on copper electrodes: the role of the kinetics of elementary steps. *Angew. Chem. Int. Ed. Engl.* **52**, 2459–2462 (2013).
101. Calle-Vallejo, F. and Koper, M. T. Theoretical considerations on the electroreduction of CO to C_2 species on Cu(100) electrodes. *Angew. Chem. Int. Ed. Engl.* **125**, 7423–7426 (2013).
102. Roldan Cuenya, B. Metal nanoparticle catalysts beginning to shape-up. *Acc. Chem. Res.* **46**, 1682–1691 (2012).
103. Ono, L. K., Croy, J. R., Heinrich, H. & Roldan Cuenya, B. Oxygen chemisorption, formation, and thermal stability of Pt oxides on Pt nanoparticles supported on SiO_2/Si(001): size effects. *J. Phys. Chem. C* **115**, 16856–16866 (2011).
104. Ono, L. K. & Roldan Cuenya, B. Formation and thermal stability of Au_2O_3 on gold nanoparticles: size and support effects. *J. Phys. Chem. C* **112**, 4676–4686 (2008).
105. Reske, R., Mistry, H., Behafarid, F., Roldan Cuenya, B. & Strasser, P. Particle size effects in the catalytic electroreduction of CO_2 on Cu nanoparticles. *J. Am. Chem. Soc.* **136**, 6978–6986 (2014).
This work unravels the particle size dependence of CO_2 electroreduction over Cu using model micelle-synthesized nanoparticles.
106. Manthiram, K., Beberwyck, B. J. & Alivisatos, A. P. Enhanced electrochemical methanation of carbon dioxide with a dispersible nanoscale copper catalyst. *J. Am. Chem. Soc.* **136**, 13319–13325 (2014).
107. Baturina, O. A. *et al.* CO_2 electroreduction to hydrocarbons on carbon-supported Cu nanoparticles. *ACS Catal.* **4**, 3682–3695 (2014).
108. Ono, L. K. & Cuenya, B. R. Effect of interparticle interaction on the low temperature oxidation of CO over size-selected Au nanocatalysts supported on ultrathin TiC films. *Catal. Lett.* **113**, 86–94 (2007).
109. Mistry, H. *et al.* Tuning catalytic selectivity at the mesoscale via interparticle interactions. *ACS Catal.* **6**, 1075–1080 (2015).
This study describes how interparticle distance and nanoparticle size can be used to control activity and selectivity during CO_2 electroreduction over Cu, providing important insights into mass transport and diffusion phenomena during this reaction on well dispersed nanostructured materials.
110. Roberts, F. S., Kuhl, K. P. & Nilsson, A. High selectivity for ethylene from carbon dioxide reduction over copper nanocube electrocatalysts. *Angew. Chem. Int. Ed. Engl.* **54**, 5179–5182 (2015).
111. Chen, C. S. *et al.* Stable and selective electrochemical reduction of carbon dioxide to ethylene on copper mesocrystals. *Catal. Sci. Technol.* **5**, 161–168 (2015).
112. Back, S., Yeom, M. S. & Jung, Active, Y. Sites of Au and Ag nanoparticle catalysts for CO_2 electroreduction to CO. *ACS Catal.* **5**, 5089–5096 (2015).
113. Mistry, H. *et al.* Exceptional size-dependent activity enhancement in the electroreduction of CO_2 over Au nanoparticles. *J. Am. Chem. Soc.* **136**, 16473–16476 (2014).
114. Gao, D. *et al.* Size-dependent electrocatalytic reduction of CO_2 over Pd nanoparticles. *J. Am. Chem. Soc.* **137**, 4288–4291 (2015).
115. Zhu, W. *et al.* Monodisperse Au nanoparticles for selective electrocatalytic reduction of CO_2 to CO. *J. Am. Chem. Soc.* **135**, 16833–16836 (2013).
116. Zhu, W. *et al.* Active and selective conversion of CO_2 to CO on ultrathin Au nanowires. *J. Am. Chem. Soc.* **136**, 16132–16135 (2014).
117. Li, C. W. & Kanan, M. W. CO_2 reduction at low overpotential on Cu electrodes resulting from the reduction of thick Cu_2O films. *J. Am. Chem. Soc.* **134**, 7231–7234 (2012).
This study introduced oxide-derived Cu as a new class of catalyst for CO_2 electroreduction with considerably improved activity at low overpotentials.
118. Tang, W. *et al.* The importance of surface morphology in controlling the selectivity of polycrystalline copper for CO_2 electroreduction. *Phys. Chem. Chem. Phys.* **14**, 76–81 (2012).
119. Chen, Y., Li, C. W. & Kanan, M. W. Aqueous CO_2 reduction at very low overpotential on oxide-derived Au nanoparticles. *J. Am. Chem. Soc.* **134**, 19969–19972 (2012).
120. Lu, Q. *et al.* A selective and efficient electrocatalyst for carbon dioxide reduction. *Nat. Commun.* **5**, 3242 (2014).
121. Sen, S., Liu, D. & Palmore, G. T. R. Electrochemical reduction of CO_2 at copper nanofoams. *ACS Catal.* **4**, 3091–3095 (2014).
122. Jia, F., Yu, X. & Zhang, L. Enhanced selectivity for the electrochemical reduction of CO_2 to alcohols in aqueous solution with nanostructured Cu–Au alloy as catalyst. *J. Power Sources* **252**, 85–89 (2014).
123. Esposito, D. V. *et al.* Low-cost hydrogen-evolution catalysts based on monolayer platinum on tungsten monocarbide substrates. *Angew. Chem. Int. Ed. Engl.* **49**, 9859–9862 (2010).
124. Bligaard, T. & Nørskov, J. K. Ligand effects in heterogeneous catalysis and electrochemistry. *Electrochim. Acta* **52**, 5512–5516 (2007).
125. Januszewska, A., Jurczakowski, R. & Kulesza, P. J. CO_2 electroreduction at bare and Cu-decorated Pd pseudomorphic layers: catalyst tuning by controlled and indirect supporting onto Au (111). *Langmuir* **30**, 14314–14321 (2014).
126. Reske, R. *et al.* Controlling catalytic selectivities during CO_2 electroreduction on thin Cu metal overlayers. *J. Phys. Chem. Lett.* **4**, 2410–2413 (2013).
127. Varela, A. S. *et al.* CO_2 electroreduction on well-defined bimetallic surfaces: Cu overlayers on Pt(111) and Pt(211). *J. Phys. Chem. C* **117**, 20500–20508 (2013).
128. Friebel, D. *et al.* Structure, redox chemistry, and interfacial alloy formation in monolayer and multilayer Cu/Au (111) model catalysts for CO_2 electroreduction. *J. Phys. Chem. C* **118**, 7954–7961 (2014).
129. Schlaup, C., Horch, S. & Chorkendorff, I. On the stability of copper overlayers on Au (111) and Au (100) electrodes under low potential conditions and in the presence on CO and CO_2. *Surf. Sci.* **631**, 155–164 (2015).
130. Kim, D., Resasco, J., Yu, Y., Asiri, A. M. & Yang, P. Synergistic geometric and electronic effects for electrochemical reduction of carbon dioxide using gold–copper bimetallic nanoparticles. *Nat. Commun.* **5**, 5948 (2014).
131. Zhao, W., Yang, L., Yin, Y. & Jin, M. Thermodynamic controlled synthesis of intermetallic Au_3Cu alloy nanocrystals from Cu microparticles. *J. Mater. Chem. A* **2**, 902–906 (2014).
132. Christophe, J., Doneux, T. & Buess-Herman, C. Electroreduction of carbon dioxide on copper-based electrodes: activity of copper single crystals and copper–gold alloys. *Electrocatalysis* **3**, 139–146 (2012).
133. Hirunsit, P. Electroreduction of carbon dioxide to methane on copper, copper–silver, and copper–gold catalysts: a DFT study. *J. Phys. Chem. C* **117**, 8262–8268 (2013).
134. Kim, D. *et al.* Insights into an autonomously formed oxygen-evacuated Cu_2O electrode for the selective production of C_2H_4 from CO_2. *Phys. Chem. Chem. Phys.* **17**, 824–830 (2015).
135. Kas, R. *et al.* Electrochemical CO_2 reduction on Cu_2O-derived copper nanoparticles: controlling the catalytic selectivity of hydrocarbons. *Phys. Chem. Chem. Phys.* **16**, 12194–12201 (2014).
136. Ren, D. *et al.* Selective electrochemical reduction of carbon dioxide to ethylene and ethanol on copper(I) oxide catalysts. *ACS Catal.* **5**, 2814–2821 (2015).
137. Verdaguer-Casadevall, A. *et al.* Probing the active surface sites for CO reduction on oxide-derived copper electrocatalysts. *J. Am. Chem. Soc.* **137**, 9808–9811 (2015).
138. Feng, X., Jiang, K., Fan, S. & Kanan, M. W. Grain-boundary-dependent CO_2 electroreduction activity. *J. Am. Chem. Soc.* **137**, 4606–4609 (2015).
139. Frese, K. W. Electrochemical reduction of CO_2 at intentionally oxidized copper electrodes. *J. Electrochem. Soc.* **138**, 3338–3344 (1991).
140. Zhang, Y.-J. & Peterson, A. A. Oxygen-induced changes to selectivity-determining steps in electrocatalytic CO_2 reduction. *Phys. Chem. Chem. Phys.* **17**, 4505–4515 (2015).
141. Le, M. *et al.* Electrochemical reduction of CO_2 to CH_3OH at copper oxide surfaces. *J. Electrochem. Soc.* **158**, E45–E49 (2011).
142. Andrews, E. *et al.* Electrochemical reduction of CO_2 at Cu nanocluster/(1010) ZnO electrodes. *J. Electrochem. Soc.* **160**, H841–H846 (2013).
143. Behrens, M. *et al.* The active site of methanol synthesis over $Cu/ZnO/Al_2O_3$ industrial catalysts. *Science* **336**, 893–897 (2012).
144. Gao, D. *et al.* pH effect on electrocatalytic reduction of CO_2 over Pd and Pt nanoparticles. *Electrochem. Commun.* **55**, 1–5 (2015).
145. Varela, A. S., Kroschel, M., Reier, T. & Strasser, P. Controlling the selectivity of CO_2 electroreduction on copper: the effect of the electrolyte concentration and the importance of the local pH. *Catal. Today* **260**, 8–13 (2016).
146. Hori, Y., Murata, A. & Takahashi, R. Formation of hydrocarbons in the electrochemical reduction of carbon dioxide at a copper electrode in aqueous solution. *J. Chem. Soc., Faraday Trans. 1* **85**, 2309–2326 (1989).
147. Murata, A. & Hori, Y. Product selectivity affected by cationic species in electrochemical reduction of CO_2 and Co at a Cu electrode. *Bull. Chem. Soc. Japan* **64**, 123–127 (1991).
148. Hori, Y., Takahashi, R., Yoshinami, Y. & Murata, A. Electrochemical reduction of CO at a copper electrode. *J. Phys. Chem. B* **101**, 7075–7081 (1997).
149. Schouten, K. J. P., Gallent, E. P. & Koper, M. T. The influence of pH on the reduction of CO and CO_2 to hydrocarbons on copper electrodes. *J. Electroanal. Chem.* **716**, 53–57 (2014).
150. Schouten, K. J. P., Gallent, E. P. & Koper, M. T. The electrochemical characterization of copper single-crystal electrodes in alkaline media. *J. Electroanal. Chem.* **699**, 6–9 (2013).
151. Koper, M. T. Theory of multiple proton–electron transfer reactions and its implications for electrocatalysis. *Chem. Sci.* **4**, 2710–2723 (2013).
152. Gupta, N., Gattrell, M. & MacDougall, B. Calculation for the cathode surface concentrations in the electrochemical reduction of CO_2 in $KHCO_3$ solutions. *J. Appl. Electrochem.* **36**, 161–172 (2006).
153. Colmati, F. *et al.* Surface structure effects on the electrochemical oxidation of ethanol on platinum single crystal electrodes. *Faraday Discuss.* **140**, 379–397 (2009).
154. Lai, S. C. & Koper, M. T. Electro-oxidation of ethanol and acetaldehyde on platinum single-crystal electrodes. *Faraday Discuss.* **140**, 399–416 (2009).
155. Colmati, F. *et al.* The role of the steps in the cleavage of the C–C bond during ethanol oxidation on platinum electrodes. *Phys. Chem. Chem. Phys.* **11**, 9114–9123 (2009).
156. Lai, S. C. & Koper, M. T. The influence of surface structure on selectivity in the ethanol electro-oxidation reaction on platinum. *J. Phys. Chem. Lett.* **1**, 1122–1125 (2010).
157. Del Colle, V., Berna, A., Tremiliosi-Filho, G., Herrero, E. & Feliu, J. Ethanol electrooxidation onto stepped surfaces modified by Ru deposition: electrochemical and spectroscopic studies. *Phys. Chem. Chem. Phys.* **10**, 3766–3773 (2008).
158. Lai, S. C. & Koper, M. T. Ethanol electro-oxidation on platinum in alkaline media. *Phys. Chem. Chem. Phys.* **11**, 10446–10456 (2009).
159. Zhou, Z. Y. *et al.* High-index faceted platinum nanocrystals supported on carbon black as highly efficient catalysts for ethanol electrooxidation. *Angew. Chem. Int. Ed. Engl.* **49**, 411–414 (2010).

160. Tian, N., Zhou, Z.-Y., Sun, S.-G., Ding, Y. & Wang, Z. L. Synthesis of tetrahexahedral platinum nanocrystals with high-index facets and high electro-oxidation activity. *Science* **316**, 732–735 (2007).
161. Tian, N., Zhou, Z.-Y., Yu, N.-F., Wang, L.-Y. & Sun, S.-G. Direct electrodeposition of tetrahexahedral Pd nanocrystals with high-index facets and high catalytic activity for ethanol electrooxidation. *J. Am. Chem. Soc.* **132**, 7580–7581 (2010).
162. Zhou, W. *et al.* Pt based anode catalysts for direct ethanol fuel cells. *Appl. Catal. B* **46**, 273–285 (2003).
163. Lamy, C., Rousseau, S., Belgsir, E., Coutanceau, C. & Léger, J.-M. Recent progress in the direct ethanol fuel cell: development of new platinum–tin electrocatalysts. *Electrochim. Acta* **49**, 3901–3908 (2004).
164. Du, W. *et al.* Platinum–tin oxide core–shell catalysts for efficient electro-oxidation of ethanol. *J. Am. Chem. Soc.* **136**, 10862–10865 (2014).
165. Erini, N. *et al.* Exceptional activity of a Pt–Rh–Ni ternary nanostructured catalyst for the electrochemical oxidation of ethanol. *ChemElectroChem* **2**, 903–908 (2015).
166. Erini, N. *et al.* Ethanol electro-oxidation on ternary platinum–rhodium–tin nanocatalysts: insights in the atomic 3D structure of the active catalytic phase. *ACS Catal.* **4**, 1859–1867 (2014).
167. Kowal, A. *et al.* Ternary Pt/Rh/SnO_2 electrocatalysts for oxidizing ethanol to CO_2. *Nat. Mater.* **8**, 325–330 (2009).
This study reports on a PtRhSnO$_2$/C ethanol electro-oxidation catalyst with high efficiency for C–C bond breaking at low overpotentials, with key insights into the mechanisms behind the improved performance of these catalysts.
168. Erini, N. *et al.* Comparative assessment of synthetic strategies toward active platinum–rhodium–tin electrocatalysts for efficient ethanol electro-oxidation. *J. Power Sources* **294**, 299–304 (2015).
169. Li, M. *et al.* Ethanol oxidation on the ternary Pt–Rh–SnO_2/C electrocatalysts with varied Pt:Rh:Sn ratios. *Electrochim. Acta* **55**, 4331–4338 (2010).
170. Du, W. *et al.* Ternary PtSnRh–SnO_2 nanoclusters: synthesis and electroactivity for ethanol oxidation fuel cell reaction. *J. Mater. Chem.* **21**, 8887–8892 (2011).
171. Li, M. *et al.* Ternary electrocatalysts for oxidizing ethanol to carbon dioxide: making Ir capable of splitting C–C bond. *J. Am. Chem. Soc.* **135**, 132–141 (2012).
172. Li, M., Liu, P. & Adzic, R. R. Platinum monolayer electrocatalysts for anodic oxidation of alcohols. *J. Phys. Chem. Lett.* **3**, 3480–3485 (2012).
173. Loukrakpam, R. *et al.* Efficient C–C bond splitting on Pt monolayer and sub-monolayer catalysts during ethanol electrooxidation: Pt layer strain and morphology effects. *Phys. Chem. Chem. Phys.* **16**, 18866–18876 (2014).

Acknowledgements
This work was supported by the US National Science Foundation (NSF-Chemistry 1213182 and NSF-DMR-1207065) and the Office of Basic Energy Sciences of the US Department of Energy (DE-FG02-08ER15995). Financial assistance from the Cluster of Excellence RESOLV at RUB (EXC 1069) funded by the Deutsche Forschungsgemeinschaft is also greatly appreciated. Portions of this work received funding from the German Federal Ministry of Education and Research (Bundesministerium für Bildung und Forschung, BMBF) under the grant #03SF0433A "MEOKATS" and #03SF0523A "CO2EKAT". S.K. acknowledges financial support by the German Research Foundation (DFG) through grant STR 596/5-1. B.R.C. and P.S. thank the European Community for partial funding under the flagship "Climate KIC/EnCO2re" program (Horizon2020).

Competing interests statement
The authors declare no competing interests.